J. Fluid Mech. (1999), *vol.* 378, *pp.* 119–143. Printed in the United Kingdom

Two-phase modelling of a fluid mixing layer

By J. GLIMM[1], D. SALTZ[1] AND D. H. SHARP[2]

[1]Department of Applied Mathematics and Statistics, University at Stony Brook, Stony Brook, NY 11794, USA

[2]Los Alamos National Laboratory, Los Alamos, NM 87545, USA

(Received 20 January 1997 and in revised form 10 July 1998)

We analyse and improve a recently-proposed two-phase flow model for the statistical evolution of two-fluid mixing. A hyperbolic equation for the volume fraction, whose characteristic speed is the average interface velocity v^*, plays a central role. We propose a new model for v^* in terms of the volume fraction and fluid velocities, which can be interpreted as a constitutive law for two-fluid mixing. In the incompressible limit, the two-phase equations admit a self-similar solution for an arbitrary scaling of lengths. We show that the constitutive law for v^* can be expressed directly in terms of the volume fraction, and thus it is an experimentally measurable quantity. For incompressible Rayleigh–Taylor mixing, we examine the self-similar solution based on a simple zero-parameter model for v^*. It is shown that the present approach gives improved agreement with experimental data for the growth rate of a Rayleigh–Taylor mixing layer.

Closure of the two-phase flow model requires boundary conditions for the surfaces that separate the two-phase and single-phase regions, i.e. the edges of the mixing layer. We propose boundary conditions for Rayleigh–Taylor mixing based on the inertial, drag, and buoyant forces on the furthest penetrating structures which define these edges. Our analysis indicates that the compatibility of the boundary conditions with the two-phase flow model is an important consideration. The closure assumptions introduced here and their consequences in relation to experimental data are compared to the work of others.

1. Introduction

Initial random disturbances at an unstable interface between fluids of distinct density lead to the formation of a chaotic mixing layer between the fluids. In the case of Rayleigh–Taylor (RT) instability, the chaotic fluid mixing is driven by an acceleration across the interface (see, e.g. Sharp 1984).

Chen *et al.* (1996) proposed a new two-phase flow model as a basis for a quantitative analysis of the statistical evolution of the mixing layer. The approach taken in formulating the model, summarized in § 2, produced striking results. The ensemble-averaged Euler equations provide a natural framework for a unified description of turbulence and two-fluid mixing. Because pressure equilibration in the two-phase flow is not imposed, several substantial improvements in the modelling are achieved: (*a*) mixing driven by pressure differences is included; (*b*) the governing two-phase equations for compressible mixing are fully hyperbolic; and (*c*) an equation of state for a mixture of immiscible fluids is not required. In this paper, we improve the formulation of the two-phase flow model and extend its range of applicability to

other interface instability problems. For the case of incompressible fluid mixing, we analyse the mathematical content and physical properties of the model, with an emphasis on its application to RT instability.

We establish five main results. The first result, discussed in § 2, is a model for the average interface velocity v^* and pressure p^*. In particular, v^* is the characteristic speed in a hyperbolic equation for the volume fraction in the two-phase flow, called the interface equation. We propose, as constitutive laws for two-fluid mixing, an expression for f^* ($f = v, p$) in terms of the volume fraction, time, and single-phase values of f.

The second result, presented in § 3, is a re-interpretation of a recently-found renormalization group fixed-point solution for incompressible RT mixing (see Glimm, Saltz & Sharp 1996). The interface equation admits self-similar solutions for an arbitrary scaling of lengths. The motion of the mixing zone edges determines the scaling law. The hyperbolicity of the interface equation represents the simple idea that surfaces of constant volume fraction are propagating entities. Thus our strategy of modelling v^* is potentially applicable to a wide range of chaotic mixing phenomena.

The third result concerns the suitability of the two-phase model for laboratory studies of chaotic fluid mixing. In the framework of self-similar incompressible mixing, the constitutive law for the average interface velocity directly determines the distributions of volume fractions and velocities across the mixing layer; v^* is, in fact, the inverse of the volume fraction profile, which is a directly observable quantity. Moreover, our theoretical analysis links the scale-invariant fluid velocities to the volume fraction. Thus any constitutive law for v^* involving only velocities and volume fractions is itself experimentally testable.

The fourth result is an analysis of the renormalization group fixed point for incompressible mixing. In § 3.2 we derive some properties of self-similar mixing which are independent of any constitutive assumptions regarding v^*. In § 3.3 we adopt a fractional linear form for v^* and give *a priori* arguments which determine all of the parameters appearing in this model in terms of the mixing coefficients α_1 and α_2. The discussion of § 4 is specific to RT instability, and it includes a preliminary comparison of the resulting volume fraction profiles with laboratory data, as well as a prediction of the expansion ratio α_2/α_1 based on an approximate model for the motion of the mixing layer centre of mass.

The fifth result, given in § 5, is an analysis of boundary conditions for the edges of the mixing layer in the ensemble-averaged flow, to complete the closure of the two-phase flow model for RT mixing. These edges correspond to the tips of the furthest penetrating structures (bubbles and spikes) in the pre-averaged flow. The boundary conditions are based on a phenomenological model for the inertial, buoyant, and drag forces on a single bubble or spike, and they supply information that is lost during the process of ensemble averaging the exact equations of motion. Phenomenological force laws for spikes and bubbles in RT mixing have been proposed by other authors. In § 5, we compare these various models, which are distinguished by their choice of phenomenological parameters, and we analyse their compatibility with two-phase flow models of RT mixing layers.

In § 6 we discuss the issue of pressure non-equilibration in the context of RT mixing. Two-pressure models of two-phase flow have been previously discussed by several authors (see, e.g. Stewart & Wendroff 1984; Holm & Kupershmidt 1984; Ransom & Hicks 1984), who have noted several desirable features of these models, including the hyperbolicity of the governing equations. In this section, we also summarize those features of our model which distinguish it from a two-phase model for RT mixing

originally proposed by Harlow & Amsden (1975) and developed further by Youngs (1984) and Freed *et al.* (1991).

The results of this paper give a simple description of a two-phase RT mixing layer that is in agreement with existing experimental data. The hyperbolic equation for the volume fraction, which to the best of our knowledge has not played a prominent role in previous studies of two-fluid mixing, appears to be of fundamental importance. In our opinion, the formulation presented here is well suited to generalizations which describe both turbulence and multiphase mixing. It is also suitable for application to practical problems, when properly interfaced with full-scale simulations. We stress that the closure relations for v^* and other average interface quantities play a crucial role in this approach. Further studies of these closure relations and the boundary conditions for the mixing layer edges are required to extend our approach to other flow regimes.

2. A two-phase flow model for a fluid mixing layer

Chen *et al.* (1996) recently proposed a two-phase flow model for fluid mixing using a formalism that is described by Drew (1983). In this section, we present this model and specify improved constitutive laws for the material coupling terms.

Effective equations of motion are derived by performing single-phase averages of the microphysical model over an infinite ensemble of microscopic flow realizations. We assume that only the z-direction is preferred in the infinite ensemble (e.g. by aligning an external acceleration along the z-axis), and that the statistics of the ensemble are translationally invariant in the transverse (x and y) directions, so that all averaged quantities depend only on z and t. One-dimensionality is imposed in practice by spatially averaging the experimental or numerical simulation data over the transverse direction(s). The ensemble-averaging process introduces new unknowns, namely second moments of fluctuating quantities and material coupling terms, which are replaced by constitutive laws. Detailed explanations of the closure models for compressible RT mixing, as well as their validation by comparison with data from two-dimensional numerical simulations, are provided by Chen (1995) and Chen *et al.* (1996).

The microphysical model that we consider is the compressible Euler equations, supplemented by a kinematic constraint for the material interface (see Drew 1983). The two-phase flow model obtained by ensemble averaging within each fluid is then

$$\frac{\partial \beta_k}{\partial t} + v^* \frac{\partial \beta_k}{\partial z} = 0, \tag{2.1}$$

$$\frac{\partial (\beta_k \rho_k)}{\partial t} + \frac{\partial (\beta_k \rho_k v_k)}{\partial z} = 0, \tag{2.2}$$

$$\frac{\partial (\beta_k \rho_k v_k)}{\partial t} + \frac{\partial (\beta_k \rho_k v_k v_k)}{\partial z} = -\frac{\partial (\beta_k p_k)}{\partial z} + \beta_k \rho_k g + p^* \frac{\partial \beta_k}{\partial z}, \tag{2.3}$$

$$\frac{\partial (\beta_k \rho_k \epsilon_k)}{\partial t} + \frac{\partial (\beta_k \rho_k v_k \epsilon_k)}{\partial z} = -p_k \frac{\partial (\beta_k v_k)}{\partial z} + (pv)^* \frac{\partial \beta_k}{\partial z}, \tag{2.4}$$

together with the constraint

$$\beta_1 + \beta_2 = 1. \tag{2.5}$$

In our notation, single-phase quantities are denoted with a subscript $k = 1, 2$; β_k, ρ_k, v_k, p_k, and ϵ_k are, respectively, the volume fraction, density, z-velocity, pressure, and specific internal energy of fluid (phase) k. A single-fluid equation of state (EOS) holds within each phase.

These equations incorporate several closure assumptions that were explained and validated by Chen (1995) and Chen *et al.* (1996), as mentioned above, namely: neglect of single-phase turbulent second moments, equality of mass-weighted and volume-weighted averages of velocity, neglect of a high-order correlation term in the energy equation, and application of the microphysical EOS to averaged variables. For the data sets studied, all of these approximations, with the exception of the zero Reynolds stress, were found to induce a negligible error. The EOS closure is, in fact, exact for EOS models based on small departures from a known reference state, such as the stiffened gas EOS (see, e.g., Menikoff & Plohr 1989), of which the polytropic EOS is a special case. We further note that (2.1)–(2.4) are derived without reference to the number of spatial dimensions in the microphysical model, although the closure approximations themselves have only been validated for two-dimensional RT mixing.

The approximations that the turbulent moments are small are closure hypotheses that reflect the physical notion that material coupling at interfaces plays a larger role than single-phase turbulence in determining the dynamics of the fluid mixing, at least in the flow regimes that were studied by Chen *et al.* While they found that the Reynolds stress is fairly small (though not negligible), they also observed that it grows over time. Fortunately, the two-phase model as derived allows alternative closures, such as a $k - \epsilon$ model or a full second-order closure in each phase, as a way to combine single-phase turbulence with two-phase mixing. This idea has been discussed by Cranfill (1991, 1992).

To fix sign conventions, we take $\rho_1 \leqslant \rho_2$, direct the external acceleration along the $+z$-direction ($g \geqslant 0$), and place the light fluid above (larger z values relative to) the heavy fluid. Altogether there are ten equations: (2.2)–(2.4) for $k = 1, 2$, two single-phase EOS models (not displayed), (2.1) for one of the phases, and (2.5). There are thirteen unknowns: in addition to the ten primitive variables β_k, v_k, ρ_k, p_k, and ϵ_k ($k = 1, 2$), there are three material coupling terms of the form $f^* \partial \beta_k / \partial z$, where $f = v$ in (2.1), p in (2.3), and pv in (2.4). We can close the system of two-phase flow equations by specifying constitutive laws for the quantities v^*, p^*, and $(pv)^*$, and boundary conditions for the edges of the mixing layer.

In relation to the microphysical ensemble, f^* ($f = v, p, pv$) is the average of the fluid quantity f, conditioned on evaluation at material interfaces; for example, p^* is the average interface pressure. Surface tension is neglected in this model, so that p^* and $(pv)^*$ are defined unambiguously. We have restored the interface averages to their exact (unclosed) form in the equations above so that we can now present improved constitutive laws for these quantities.

The height at which β_1 (β_2) vanishes is labelled the lower (upper) edge of the mixing zone, and it corresponds to the tip of the frontier portion of light (heavy) fluid in the microscopic flow. Therefore f^* must equal f_1 (f_2) at the lower (upper) edge of the mixing zone. For the cases $f = v$ and $f = p$, we make two assumptions about the form of a constitutive law for f^*: (*a*) f^* is a linear combination of f_1 and f_2; and (*b*) the coefficients of f_1 and f_2 depend on volume fraction and time. These assumptions imply an interpolation formula for f^* of the form

$$f^* = \mu_1^f(t, \beta_1) f_2 + \mu_2^f(t, \beta_2) f_1, \tag{2.6}$$

where $\mu_k^f(t, \beta_k = 0) = 0$ and $\mu_k^f(t, \beta_k = 1) = 1$ for $k = 1, 2$, in order to satisfy the boundary conditions for f^* stated above. The constitutive law for $(pv)^*$ is more complicated, due to the fact that pv is a nonlinear function of primitive variables, and it is discussed in detail elsewhere (see Glimm, Saltz & Sharp 1998*b*).

Equation (2.6) is proposed as a useful starting point for the constitutive modelling of two-fluid mixing. It is based on the hypothesis that an average interface quantity is given as some unspecified weighted average of its single-phase values. At a height z and time t, the contribution to $f^*(z, t)$ from phase $3 - k$ ($k = 1, 2$) is weighted according to how much of the *other* fluid there is, as indicated by the volume fraction $\beta_k(z, t)$.

In the model for the average interface velocity, Galilean frame invariance imposes an algebraic constraint on the coefficients μ_k^v. If we require (2.6) for $f = v$ to hold in a coordinate system moving vertically with a constant velocity v_o, then

$$v^* - v_o = \mu_1^v(t, \beta_1)(v_2 - v_o) + \mu_2^v(t, \beta_2)(v_1 - v_o).$$

Since v_o is arbitrary, it follows that

$$\mu_1^v(t, \beta_1) + \mu_2^v(t, \beta_2) = 1 \tag{2.7}$$

for $0 \leqslant \beta_1 \leqslant 1$, $\beta_2 = 1 - \beta_1$. In the incompressible limit, pressure is defined to within an arbitrary additive constant p_o, so that

$$p^* - p_o = \mu_1^p(t, \beta_1)(p_2 - p_o) + \mu_2^p(t, \beta_2)(p_1 - p_o).$$

Again, since p_o is arbitrary, it follows that

$$\mu_1^p(t, \beta_1) + \mu_2^p(t, \beta_2) = 1 \tag{2.8}$$

for $0 \leqslant \beta_1 \leqslant 1$, $\beta_2 = 1 - \beta_1$.

Equation (2.6) is a generalization of the original model for the average interface quantities that was proposed by Chen *et al.* (1996). They set $\mu_k^f(t, \beta_k) = \beta_k$ for $f = v$, p, pv and $k = 1, 2$, and compared $f^* \partial \beta_k / \partial z$ to its exact value evaluated from two-dimensional RT simulation data covering a fairly wide range of fluid conditions. Agreement was good for $f = v$ and $f = pv$ and excellent for $f = p$. Glimm *et al.* (1996) showed that for incompressible fluid mixing, this choice of interpolation scheme for v^* constrains the volume fractions and two-phase velocities to vary linearly across the mixing region. The actual variation in these quantities has not been adequately established. Freed *et al.* (1991) displayed a monotone, slightly convex polynomial fit to several volume fraction profiles. Chen *et al.* (1993) reported a region of non-monotonicity in the volume fraction profile, situated well inside the mixing layer. As we discuss in § 4, there are also ambiguities associated with locating the edges of the mixing zone in simulations and experiments, possibly due to the effects of a finite sample size or a lack of perfect scale invariance. Furthermore, the analysis of § 3.1 shows that if $\mu_1^v(t, \beta) = \mu_2^v(t, \beta)$ in incompressible flow, then the mixing zone is constrained to expand at the same rate in each direction. Thus there are uncertainties as to the appropriate choice of the coefficients μ_k^f, and correct modelling of these quantities is a key problem.

The equations of motion form a natural two-phase extension of the Euler equations for compressible fluid flow in an external force field, with the addition of the interface equation (2.1) and source terms representing the interchange of momentum and energy between the phases. One can easily confirm that (2.1)–(2.4) are hyperbolic, with characteristic speeds v_k and $v_k \pm c_k$ for each phase and v^* for the interface mode. It is evident that the characteristic structure of the system changes across any surface

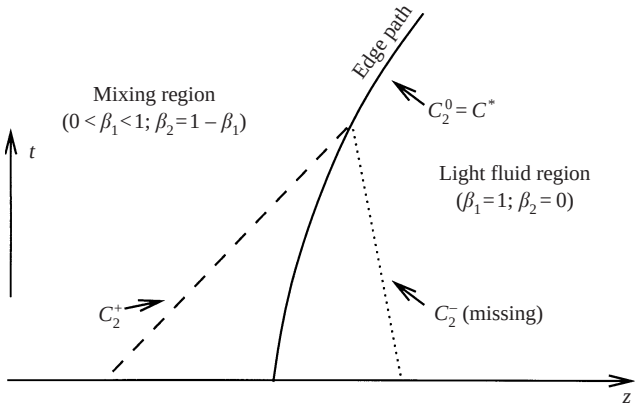

FIGURE 1. The method of characteristics for the heavy phase applied at the upper edge of the mixing zone in compressible two-phase mixing. The C^* and C_2^0 characteristics, corresponding to the interface and heavy fluid particle modes, respectively, coincide with the path of the upper edge. The left-facing sound mode in the heavy phase, C_2^-, is missing, as it originates from outside the mixing layer, where there is no heavy fluid.

on which one of the volume fractions vanishes, because the number of characteristics and the system size changes at each edge of the mixing layer. Moreover, the equations are incomplete there, as there is no incoming sound wave for the phase of vanishing volume fraction. This situation is illustrated in figure 1. In the example shown in this figure, the interface and heavy particle characteristics, respectively labelled C^* and C_2^0, coincide with the trajectory of the upper edge of the mixing zone. The right-facing sound characteristic in the heavy phase is labelled C_2^+ and emanates from the interior of the mixing zone. The left-facing sound characteristic in the heavy phase is labelled C_2^- and emanates from outside the mixing zone, where there is no heavy fluid. Thus there is no C_2^- characteristic at the upper edge; by a similar argument, there is no C_1^+ characteristic at the lower edge.

In our interpretation, the missing characteristics indicate that some information about the physical behaviour of the leading coherent structures in the pre-averaged flow is represented by the motion of the mixing zone boundaries in the two-phase flow. In the case of RT mixing, these structures (or modes) are the tips of the leading spikes and bubbles. We can supply this missing information, and therefore close the system of equations, by formulating dynamical equations for the trajectories of the mixing zone edges. This issue is discussed in § 5.

In the incompressible limit, the RT mixing zone edges are known from experiment (Read 1984; Youngs 1989) and theory (Glimm & Sharp 1990) to follow constant-acceleration trajectories given by

$$Z_1(t) = -\alpha_1 A g t^2, \quad Z_2(t) = \alpha_2 A g t^2, \tag{2.9}$$

where Z_k is the position of the edge corresponding to the limit of vanishing β_k, $A = (\rho_2 - \rho_1)/(\rho_2 + \rho_1)$ is the Atwood density ratio, and α_1 and α_2 are positive mixing coefficients that can depend on A. As shown in the following section, these trajectories lead to self-similar solutions to the incompressible continuity and interface equations that are complete up to specification of α_1 and α_2. An additional modelling assumption, described in § 4.3, leads to a prediction of α_2/α_1 as a function of A, which can be compared to experimental data.

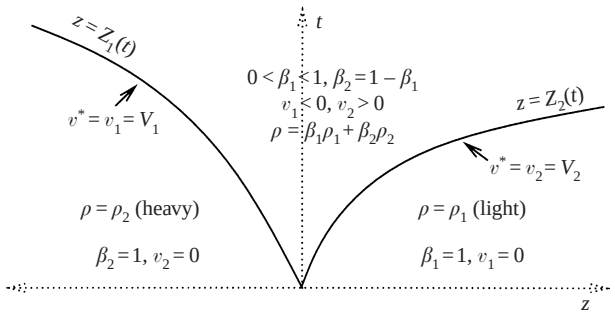

FIGURE 2. Incompressible two-phase mixing in the (z, t)-plane, showing the range and boundary values of the fluid volume fractions and velocities.

3. Incompressible two-phase mixing

The main assumptions of this section are the interface (2.1) and two-phase continuity (2.2) equations, incompressibility, and the v^* closure. Following Glimm *et al.* (1996), we average the incompressible continuity condition $\nabla \cdot \boldsymbol{v}$ within each phase and apply the definition of v^* to obtain

$$\frac{\partial \beta_k v_k}{\partial z} = v^* \frac{\partial \beta_k}{\partial z}. \tag{3.1}$$

The v^* closure depends on the coefficients μ_k^f in the constitutive law (2.6) for $f = v$, which we restate here without the superscript v,

$$v^* = \mu_1(t, \beta_1) v_2 + \mu_2(t, \beta_2) v_1. \tag{3.2}$$

This equation reduces the modelling of v^* to the specification of the coefficients μ_k. In § 3.3 we assign μ_k a parametric form and then determine all of the free parameters in this form from boundary data.

The boundary data that we assume here are specified as the location $Z_k(t)$ of the mixing zone edges, or equivalently as the edge velocities $V_k(t) = \mathrm{d}Z_k/\mathrm{d}t$. The only assumption that we make regarding the motion of the edges is that $V_1 < 0$ and $V_2 > 0$, which expresses the idea that the mixing zone expands.

The main result of § 3.1 is a complete closed-form solution of the continuity and interface equations in terms of initial and boundary data, and also in terms of the μ_k of (3.2). This solution is made more precise as the initial and boundary data are given more explicitly, first to satisfy self-similar hypotheses in § 3.2, and then with μ_k uniquely specified in terms of the boundary data, i.e. the proportionality constants for the edge trajectories, in § 3.3.

The assumed form for v^* allows the decoupling of the continuity equations from the momentum equations and is thus critical in our ability to integrate the continuity equations in closed form. Thus we see the physical implications of the v^* closure (3.2). The transfer of momentum in the interior of the mixing zone does not influence the volume fraction and velocity profiles, while these quantities do depend on momentum transfer at the edges. The role of the momentum equations is therefore to influence the boundary data. Integrated (centre of mass) momentum and other quantities are analysed in § 3.2 for the purpose of constraining the boundary data and also to facilitate comparison to experimental data.

The geometry of the mixing zone is illustrated schematically in figure 2.

3.1. *Solution of continuity and interface equations*

The purpose of this subsection is to provide a closed-form solution for the velocities v_1, v_2, and v^* in terms of the volume fraction. The solution for v_k, when substituted into the continuity equation (2.2), yields a hyperbolic conservation law for β_k alone which has a unique smooth solution for the given boundary data (see Glimm *et al.* 1998*b*). We thereby demonstrate that the volume fraction and velocity profiles follow directly from a constitutive law for v^* and boundary conditions for the mixing zone edges.

We first derive an expression for the velocity as a function of volume fraction, which, by substitution, leads to a hyperbolic conservation law for β_k. Summing (3.1) over k and using (2.5),

$$\frac{\partial}{\partial z}(\beta_1 v_1 + \beta_2 v_2) = 0. \tag{3.3}$$

The solution to this ordinary differential equation (ODE) is $\beta_1 v_1 + \beta_2 v_2 = U(t)$. In the light (heavy) fluid region outside the mixing zone, conservation of mass is simply $\partial v_1/\partial z = 0$ ($\partial v_2/\partial z = 0$). Since v_1 (v_2) must be continuous across the upper (lower) mixing zone edge, where $\beta_2 = 0$ ($\beta_1 = 0$), it follows that v_1 (v_2) is uniform and equal to $U(t)$ in the light (heavy) fluid region. Chaotic fluid mixing occurs in a finite but large domain, for which there is a boundary condition that $v_1 = 0$ ($v_2 = 0$) at the upper (lower) wall. It follows that $U = 0$ in a domain of arbitrary but finite size; hence $U = 0$ in general. Enforcing continuity of the dependent variables at the mixing zone edges, it follows that

$$\beta_1 v_1 + \beta_2 v_2 = 0. \tag{3.4}$$

At any given time, (3.1) is equivalent to an ODE relating the variation in β_k and v_k across the mixing region,

$$\frac{\mathrm{d}v_k}{\mathrm{d}\beta_k} = \frac{v^* - v_k}{\beta_k}. \tag{3.5}$$

Let $k' = 3 - k$ be the complementary index to k. Using the model (3.2) for v^* in conjunction with (2.7) and (3.4) to eliminate $v_{k'}$ from (3.5), we obtain

$$-\frac{1}{v_k}\frac{\mathrm{d}v_k}{\mathrm{d}\beta_k} = \left[\frac{\mu_k^v(t,\beta_k)}{\beta_k} - \frac{\mu_{k'}^v(t,\beta_{k'})}{\beta_{k'}} + \frac{1}{\beta_{k'}}\right], \tag{3.6}$$

The boundary conditions for this ODE are

$$\beta_k = 0, \quad v_k = V_k, \quad v_{k'} = 0 \quad \text{at } z = Z_k(t),$$

$$\mu_k(t,0) = 0, \quad \mu_k(t,1) = 1,$$

for $k = 1, 2$. The solution to (3.6) is then

$$v_k = V_k \beta_{k'} \mathrm{e}^{-F_k(t,\beta_k)}, \tag{3.7}$$

where

$$F_k(t,\beta_k) = \int_0^{\beta_k} \left[\frac{\mu_k(t,\phi_k)}{\phi_k} - \frac{\mu_{k'}(t,\phi_{k'})}{\phi_{k'}}\right] \mathrm{d}\phi_k. \tag{3.8}$$

In this integral the constraint $\phi_k + \phi_{k'} = 1$ holds. It follows from (3.7) that v_1 and v_2 do not change sign inside the mixing zone; hence $v_1 < 0$ and $v_2 > 0$ in this region.

We now derive a constraint relating the ratio of the edge velocities to the μ_k. Solving (3.5) for v^* and using (3.6) to substitute for $\mathrm{d}v_k/\mathrm{d}\beta_k$,

$$v^* = [\beta_{k'}\mu_{k'}(t,\beta_{k'}) - \beta_k\mu_k(t,\beta_k)]\,\frac{v_k}{\beta_{k'}}. \tag{3.9}$$

The right-hand side of this expression must give the same v^* for both $k = 1$ and $k = 2$. This condition can be written as

$$0 = [\beta_2\mu_2(t,\beta_2) - \beta_1\mu_1(t,\beta_1)]\,\frac{\beta_1 v_1 + \beta_2 v_2}{\beta_1\beta_2},$$

and it is clearly satisfied inside the mixing region ($0 < \beta_k < 1$) due to the incompressibility relation (3.4). At the lower edge of the mixing zone, we need

$$0 = V_1 + \lim_{\beta_1 \to 0} \frac{v_2}{\beta_1}.$$

Using the velocity solution (3.7), this expression is equivalent to $V_1 = -V_2 \mathrm{e}^{-F_2(t,1)}$; similarly, at the upper edge we have $V_2 = -V_1 \mathrm{e}^{-F_1(t,1)}$. Since $F_1(t,1) = -F_2(t,1)$, it follows that these edge constraints are identical and equivalent to

$$\left|\frac{V_2}{V_1}\right| = \mathrm{e}^{-F_1(t,1)}. \tag{3.10}$$

3.2. *Self-similar mixing*

In this subsection, we study self-similar incompressible solutions of (2.1), (2.2) and (2.5). We show that v^* is the inverse to β_k as a function of z. This analysis does not assume (3.2) or any other form of closure for v^*. As a result, (3.2) or any other model is experimentally testable by comparison to results of this section. We also derive other experimentally testable consequences of self-similarity and incompressibility.

To define self-similarity, we introduce a length scale $\mathscr{Z}(t)$ and its derivative, $\mathscr{V}(t) = \mathrm{d}\mathscr{Z}/\mathrm{d}t$, and assume proportionality of all lengths in the problem to $\mathscr{Z}$, so that

$$Z_k(t) = (-1)^k \alpha_k \mathscr{Z}(t), \quad V_k(t) = (-1)^k \alpha_k \mathscr{V}(t). \tag{3.11}$$

For RT instability, $\mathscr{Z}(t) = Agt^2$. Equations (3.11) define the (positive) mixing coefficients α_1 and α_2. Self-similarity requires the initial data $\mathscr{Z}(0) = 0$, which approximates a mixing layer that is negligibly thin, and hence self-similar, at $t = 0$. This assumption is satisfied to a reasonably degree in the RT experiments of Read (1984) and Youngs (1989).

We define a scaled position, $\hat{z} = z/\mathscr{Z}$, and a scaled velocity, $\hat{v} = v/\mathscr{V}$. We substitute the similarity form $\beta_k(z,t) = \beta_k(\hat{z})$ into the interface equation (2.1) and multiply by $\mathscr{Z}/\mathscr{V}$, which gives

$$(-\hat{z} + \hat{v}^*)\frac{\mathrm{d}\beta_k}{\mathrm{d}\hat{z}} = 0.$$

If the volume fraction profile has no flat portion inside the mixing zone, then this ODE can be satisfied only by setting the quantity in parentheses equal to zero,

$$\hat{z} = \hat{v}^*. \tag{3.12}$$

Thus $\hat{v}^*$, as a function of volume fraction, is simply the inverse of the volume fraction profile.

The velocities $\widehat{v}_1$ and $\widehat{v}_2$ likewise are determined directly from the volume fraction. Substituting (3.12) into the ODE (3.1) for $k = 1$ and integrating with respect to β_1,

$$\beta_1 \widehat{v}_1 = \int_0^{\beta_1} \widehat{z}(\beta_1')\, \mathrm{d}\beta_1', \tag{3.13}$$

while $\beta_2 \widehat{v}_2 = -\beta_1 \widehat{v}_1$, due to (3.4). Applying the boundary condition that $v_1 = 0$ at the upper edge, (3.13) implies that

$$\int_0^1 \widehat{z}(\beta_1)\, \mathrm{d}\beta_1 = 0, \tag{3.14}$$

which is an 'Equal Area Rule' for the inverse volume fraction profile.

The Equal Area Rule is a consequence of the assumptions of incompressibility and self-similarity, and it must hold regardless of the specific form of v^*. Since volume fraction profiles are measurable (Youngs 1989; Snider & Andrews 1994), this rule is a useful check on the self-similarity of the mixing which is directly applicable to experimental data. Moreover, even though measured velocities are currently unavailable, the combination of (3.4), (3.12) and (3.13) shows that all of the velocity profiles can be determined from volume fraction data. In fact, velocity profiles can be inferred even when the mixing is not self-similar, provided that two volume fraction profiles closely spaced in time are available (Glimm, Saltz & Sharp 1998*a*). Therefore, any constitutive law for v^* involving only the volume fractions and velocities can be tested using available experimental methods.

The possibility that there is a finite segment of constant β_k in the mixing zone is not considered here. We also note that (3.12) makes sense provided that v^* increases from the lower edge to the upper edge of the mixing layer; otherwise, (2.2) admits discontinuous self-similar solutions.

We next derive identities for transverse-averaged system quantities, which will serve to constrain possible boundary conditions. First note that the total mass M of the mixing layer depends only on the rate at which mass enters the mixing region,

$$M(t) = M(0) + \rho_1[Z_2(t) - Z_2(0)] + \rho_2[Z_1(0) - Z_1(t)].$$

It follows from the assumed initial data, $Z_k(0) = 0$ (hence $M(0) = 0$), the identities

$$\frac{\rho_k}{\rho_2 + \rho_1} = \tfrac{1}{2}\left[1 + (-1)^k A\right], \tag{3.15}$$

and (3.11) that

$$\widehat{M} = \tfrac{1}{2}(1 + A)\alpha_1 + \tfrac{1}{2}(1 - A)\alpha_2, \tag{3.16}$$

where $\widehat{M} = M/(\rho_2 + \rho_1)\mathscr{Z}(t)$. The total momentum P of the mixing layer is given by

$$P(t) = \int_{Z_1(t)}^{Z_2(t)} (\beta_1 \rho_1 v_1 + \beta_2 \rho_2 v_2)\, \mathrm{d}z.$$

Replacing $\beta_1 v_1$ with $-\beta_2 v_2$, transforming to scaled variables, and using (3.15), we obtain

$$\widehat{P} = A \int_{-\alpha_1}^{\alpha_2} \beta_2 \widehat{v}_2\, \mathrm{d}\widehat{z}, \tag{3.17}$$

where $\widehat{P} = P/(\rho_2 + \rho_1)\mathscr{Z}(t)\mathscr{V}(t)$. Equation (3.17) shows that $\widehat{P}$ is positive definite for $A \neq 0$; in other words, the total momentum of the mixing layer has a preferred

direction of increase regardless of the densities of the fluids or the velocities of the edges.

The centre-of-mass position Z is given by

$$Z(t) = \frac{1}{M}\int_{Z_1(t)}^{Z_2(t)} (\beta_1\rho_1 + \beta_2\rho_2) z \, \mathrm{d}z.$$

We cast this integral in scaled variables and evaluate it partially to obtain

$$\widehat{M}\widehat{Z} = \tfrac{1}{4}(1+A)(\alpha_2^2 - \alpha_1^2) - A\int_{-\alpha_1}^{\alpha_2} \beta_1 \widehat{z} \, \mathrm{d}\widehat{z}, \tag{3.18}$$

with $\widehat{Z} = Z/\mathscr{Z}(t)$. For the centre-of-mass velocity $V = \mathrm{d}Z/\mathrm{d}t$, we have $\widehat{V} = \widehat{Z}$, with $\widehat{V} = V/\mathscr{V}(t)$. Even though the fluids are incompressible, $P \neq MV$ because the density $\rho = \beta_1\rho_1 + \beta_2\rho_2$ is variable. Furthermore, the centre of mass can remain stationary or move backward in spite of the fact that the mixing layer momentum is forward.

Integrating by parts in (3.18), we can write $\widehat{Z}$ in terms of α_1, α_2, A, and an integral over the square of the inverse volume fraction profile,

$$\widehat{M}\widehat{Z} = \tfrac{1}{4}(1-A)\alpha_2^2 - \tfrac{1}{4}(1+A)\alpha_1^2 + \tfrac{1}{2}A\int_0^1 \widehat{z}^2 \, \mathrm{d}\beta_1. \tag{3.19}$$

3.3. *A v^* closure unique in terms of α_1 and α_2*

In this subsection, we propose a specific form for the coefficients μ_k in (3.2) and derive closed-form expressions for the self-similar distributions of volume fractions and velocities. In § 4, we examine these solutions for the case of RT instability.

We propose for μ_k the fractional linear form

$$\mu_k(t, \beta_k) = \frac{a_k\beta_k + d_k\beta_{k'}}{c_k\beta_k + b_k\beta_{k'}}, \tag{3.20}$$

for $k = 1, 2$, where the a_k, b_k, c_k and d_k are time-dependent coefficients to be determined. Equation (3.20) can be understood as the first-order step in a systematic determination of μ_k by the method of Padé approximation. Applying the boundary conditions on μ_k, it is clear that $d_k = 0$ and $c_k = a_k$. Furthermore, the numerator and denominator in (3.20) can be multiplied by any non-zero number without changing the value of μ_k, so that we are free to set either a_k or b_k arbitrarily, for each k. It convenient to choose $a_1 = \alpha_1$ and $a_2 = \alpha_2$, and we are left with two undetermined coefficients b_1 and b_2.

There are two mathematical constraints on the μ_k, namely (2.7) and (3.10). Under the assumption of self-similar flow, the ratio of the edge velocities is time independent with magnitude α_2/α_1. Therefore neither constraint involves t explicitly, so we can omit it from the following equations. Evaluating (3.8) for $F_1(1)$ and inserting the result into (3.10), we have

$$\left(\frac{b_1}{\alpha_1}\right)^{\frac{\alpha_1}{\alpha_1 - b_1}} \left(\frac{b_2}{\alpha_2}\right)^{\frac{\alpha_2}{b_2 - \alpha_2}} = \frac{\alpha_2}{\alpha_1}, \tag{3.21}$$

while (2.7) implies the simple relation

$$b_1 b_2 = \alpha_1\alpha_2. \tag{3.22}$$

The unique solution to the two equations (3.21) and (3.22) for the two unknowns b_1

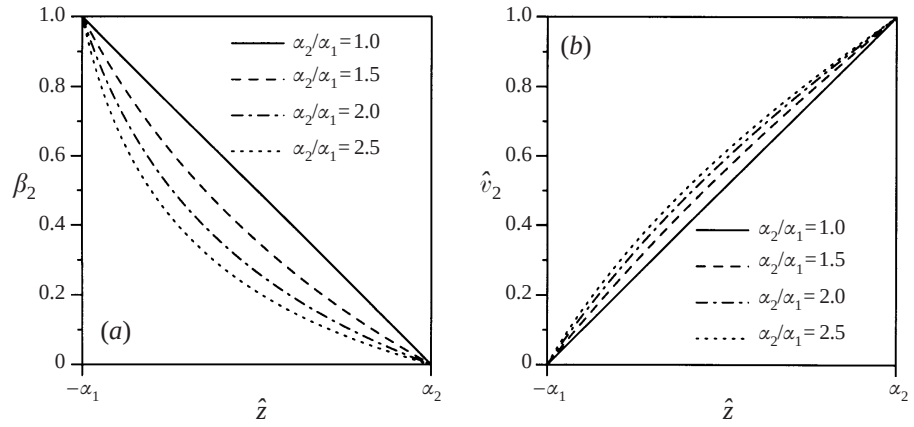

FIGURE 3. Scale-invariant heavy fluid volume fraction and velocity profiles for different values of the mixing layer expansion ratio α_2/α_1. The vertical axis in (*a*) is the volume fraction of heavy fluid β_2, which varies from 1 at the lower edge to 0 at the upper edge of the mixing zone. The vertical axis in (*b*) is the scaled heavy fluid velocity $\hat{v}_2$, defined in § 3.2, which varies from 0 at the lower edge to α_2 at the upper edge of the mixing zone. The horizontal axis in each graph is the scaled height $\hat{z}$, defined in § 3.2, which varies from $-\alpha_1$ at the lower edge to α_2 at the upper edge.

and b_2 is

$$b_1 = \alpha_2, \quad b_2 = \alpha_1,$$

and our final proposed model is then

$$\mu_k = \frac{\alpha_k \beta_k}{\alpha}, \tag{3.23}$$

where $\alpha \equiv \alpha_1\beta_1 + \alpha_2\beta_2$.

It is easy to show that $e^{-F_k(\beta_k)} = \alpha_{k'}/\alpha$, and with this expression we finally obtain a two-parameter (α_1, α_2) family of self-similar solutions from (3.7) and (3.12),

$$\hat{v}_1 = -\frac{\alpha_1\alpha_2\beta_2}{\alpha}, \quad \hat{v}_2 = \frac{\alpha_1\alpha_2\beta_1}{\alpha}, \tag{3.24}$$

$$\hat{z} = \left(\beta_1^2\alpha_1 - \beta_2^2\alpha_2\right)\frac{\alpha_1\alpha_2}{\alpha^2}. \tag{3.25}$$

Combining (3.2) and (3.23), we find a fully explicit expression for v^*, which is

$$v^* = \frac{\alpha_1\beta_1 v_2 + \alpha_2\beta_2 v_1}{\alpha_1\beta_1 + \alpha_2\beta_2}. \tag{3.26}$$

Note that this family of self-similar solutions is independent of the choice of scaling law $\mathscr{Z}(t)$. When the mixing is not self-similar (i.e. arbitrary edge velocities), μ_k, v_k, and v^* have explicit solutions in terms of the V_k and β_k that are straightforward generalizations of the corresponding equations given above (see Glimm *et al.* 1998*a*). The inverse volume fraction $z(t, \beta_k)$, on the other hand, can be expressed only in terms of a time integral of v^*.

In figure 3, we display the volume and velocity profiles given by (3.25) and (3.24) for different values of α_2/α_1.

4. Incompressible Rayleigh–Taylor mixing

In this section we discuss features of the incompressible self-similar solution that are specific to RT flow. Section sec:RT:profiles compares the profiles predicted by the fractional linear model to those determined by experiment and by simulation and two-phase flow models of other authors. In § 4.2 we discuss pressure boundary conditions for incompressible RT mixing. In § 4.3 we study the centre-of-mass motion of the RT mixing layer, and then introduce a further hypothesis which allows a direct comparison of the model to experimental data for the expansion ratios α_2/α_1. Section 4.4 contains some comments regarding the distinction between the model for v^* studied here and the one originally proposed by Chen *et al.*

4.1. *Volume fraction and velocity profiles*

For the case of RT instability, α_1 is approximately universal and equal to 0.06 (Youngs 1989), while α_2 equals α_1 at $A = 0$ and then increases slowly with increasing A, reaching roughly $2\alpha_1$ at $A = 0.9$, according to experimental data (Youngs 1989). Volume fraction profiles computed from (3.25) for α_2/α_1 ranging from 1.0 to 2.5 are displayed in figure 3(*a*).

By definition, the mixing zone edge in the macroscopic flow corresponds to the tip of the furthest penetrating coherent mode in the microscopic flow. In the Rayleigh–Taylor literature, there are two common methods for determining the edge position from experimental or simulation data: (*a*) apply the definition literally; e.g. measure the position of the bubble edge as the height of the tip of the furthest penetrating bubble; or (*b*) determine the self-similar distribution of volume fraction and then consider the edges to be where the vanishing phase has dropped to, say, a 5% volume fraction. Method (*a*) was apparently followed in Read's (1984) and Youngs' (1989) measurements of the mixing coefficients (see, e.g. figure 8 of Read 1984), as well as in front-tracking simulations of RT instability (Glimm *et al.* 1990; Chen *et al.* 1993). Method (*b*) was applied to experimental data by Snider & Andrews (1994) and simulation data by Freed *et al.* (1991).

Measured volume fraction profiles tend to tail off slowly near the edges of the mixing layer. It has not been adequately established whether this feature indicates a real property of the self-similar, ensemble-averaged mixing or, alternatively, a deviation from perfect scale invariance, a distortion due to a finite sample size, or simply experimental uncertainty. If the tailing off in the profiles is a real feature of the self-similar, ensemble-averaged two-phase flow, then the corresponding physical property is that the volume fractions are smooth, and hence $\mathrm{d}\beta_k/\mathrm{d}\hat{z} = 0$, at the mixing zone edges. As shown in figure 3(*a*), (3.25) gives only convex volume fraction profiles, and it is easy to show mathematically that there is no self-similar solution within the class of fractional linear v^* which satisfies $\mathrm{d}\beta_k/\mathrm{d}\hat{z} = 0$ at the edges. Thus a comparison between theoretical and experimental volume fraction profiles depends on how one interprets the data near the mixing zone edges.

Youngs (1989) and Snider & Andrews (1994) show some self-similar distributions of volume fraction that were measured at low A. Away from the rounded region near each mixing zone edge, all of these profiles are linear, in agreement with the $\alpha_2/\alpha_1 = 1$ profile shown in figure 3(*a*). In fact, Snider & Andrews extrapolate the linear portion of their profiles to $\beta_k = 0$ and 1, as an alternative scheme for locating the mixing zone edges, and they demonstrate that this method gives consistent values of α_1. We interpret this result as suggesting that the tailing off in the profiles does not appear in the RNG fixed point solution.

The β_2 curves shown in figure 3(*a*) and the $\hat{v}_2$ curves shown in figure 3(*b*) agree

qualitatively with the predictions of the two-phase model of Freed *et al.* (1991), in that they are convex and concave across the mixing region, respectively, with the amount of curvature in the profiles increasing with increasing α_2/α_1 and the β_2 profile more strongly curved than the $\widehat{v}_2$ profile at each α_2/α_1. Freed *et al.* also claim to have agreement with the results of their direct numerical simulations, within the accuracy of their simulation data, and they show a completely convex polynomial fit to the self-similar volume fraction profiles in one of their simulations. It is not clear whether the shape of this curve indicates the absence of a tail in the statistically-averaged simulation data, or is a result of fitting the data to a low-degree polynomial. The volume fraction profiles obtained from these simulations are considerably noisier than their counterparts in experiments (Chen *et al.* 1993; Freed *et al.* 1991; Snider & Andrews 1994; Youngs 1989).

Experimentally determined velocity profiles are not available. However, as we mentioned in the previous section, the scale-invariant velocities $\widehat{v}_1$, $\widehat{v}_2$, and $\widehat{v}^*$ can be determined directly from volume fraction data; in particular, $\widehat{v}^* = \widehat{z}$ and is therefore the inverse of the volume fraction profile. We emphasize the following points: within the framework of self-similar incompressible mixing, (*a*) the only approximation in our solution for the β_k and v_k is in the form of a closure relation for v^*; and (*b*) any such closure relation involving only velocities and volume fractions is testable with current experimental techniques.

There will eventually be enough data to resolve the issue of whether or not the volume fraction is smooth at the edges of the mixing zone. Such data will then suggest a reasonable functional form for $\beta_k(\widehat{z})$, parametrized by α_1 and α_2. Subsequently, one can work backwards using the procedure described in § 3 to determine the coefficients μ_k in the constitutive law (3.2) for v^*. We believe that this approach will be useful, as we expect that future studies will show the closure framework proposed here to be applicable in a broader framework than just incompressible self-similar mixing.

4.2. *Pressure boundary conditions*

The solution of the momentum conservation equations (2.3) for the case of incompressible two-phase flow is addressed in a recently completed paper (Glimm *et al.* 1998*b*). We have already mentioned some challenging aspects of this problem in § 2, namely the closure relation for p^* and the possible inclusion of the single-phase Reynolds stress. Another important point is that although the drag/buoyancy boundary conditions that are proposed in § 5 are sufficient to close the two-phase equations for compressible mixing, there is still incomplete information in the incompressible limit even when the mixing zone edge trajectories are known. In this subsection, we determine boundary conditions for the pressures p_1 and p_2.

Considering the RT mixing layer as a moving entity, we write Newton's Law as

$$\frac{\mathrm{d}P}{\mathrm{d}t} = Mg - \Delta p, \tag{4.1}$$

where the notation for the centre-of-mass variables and their scaled versions was introduced in the previous section and Δp is the net downward pressure force on the mixing zone boundaries,

$$\Delta p(t) = p_1\,(Z_2(t), t) - p_2\,(Z_1(t), t)\,. \tag{4.2}$$

Of course, (4.1) also follows directly from integrating the momentum equations (2.3). It is advantageous to write Newton's Law in terms of scaled variables, which are time

independent. Since $P = (\rho_2 + \rho_1)\mathscr{L}\mathscr{V}\widehat{P}$ and $\mathscr{L}(t) = Agt^2$,

$$\frac{\mathrm{d}P}{\mathrm{d}t} = 6(\rho_2 - \rho_1)A(gt)^2\widehat{P},$$

with $\widehat{P} = P/2(\rho_2 - \rho_1)Ag^2t^3$. Newton's Law then takes the time-independent form

$$6A\widehat{P} = \widehat{M} - \Delta\widehat{p}, \tag{4.3}$$

where $\Delta\widehat{p} = \Delta p/(\rho_2 - \rho_1)(gt)^2$.

At $t = 0$, the fluids are at rest and the mixing zone is a point at the origin of the (z,t)-plane, as described in § 3. The pressure fields are hydrostatically distributed relative to the pressure p_i at the position of the undisturbed interface,

$$\begin{aligned} p_1(z,0) &= p_i + \rho_1 gz \quad \text{for } z > 0, \\ p_2(z,0) &= p_i + \rho_2 gz \quad \text{for } z < 0. \end{aligned}$$

Because there is no fluid motion in the pure-phase regions as the incompressible two-phase flow evolves, one might expect that the pressures outside the mixing zone remain unchanged. We label this situation with a superscript h, i.e.

$$\begin{aligned} p_1(z,t) = p_1^h(z,t) &= p_i + \rho_1 gz \quad \text{for } z > Z_2(t), \\ p_2(z,t) = p_2^h(z,t) &= p_i + \rho_2 gz \quad \text{for } z < Z_1(t). \end{aligned}$$

Enforcing continuity of pressure across a mixing zone boundary, it follows that $\Delta p^h(t) = \rho_1 g Z_2(t) - \rho_2 g Z_1(t)$; equivalently,

$$\Delta\widehat{p}^h = \tfrac{1}{2}(1 + A)\alpha_1 + \tfrac{1}{2}(1 - A)\alpha_2.$$

Comparing to (3.16), we see that $\Delta\widehat{p}^h = \widehat{M}$. Thus, if $\Delta\widehat{p} = \Delta\widehat{p}^h$, then Newton's Law (4.3) implies that there is no net force on the mixing layer, so that $\widehat{P} = 0$ for $A \neq 0$. Such a conclusion contradicts the observation made in § 3.2 that $\widehat{P}$ is positive definite for $A \neq 0$. It follows that the pressure in at least one of the pure-phase regions must vary over time, in spite of the fact that there is no fluid motion in this region.

Newton's Law actually gives $\Delta\widehat{p}$ as a function of α_1 and α_2, since the other quantities appearing in (4.3) are determined from (3.16) and (3.17). Since our model has two distinct pressures, there remains a missing pressure boundary condition for the incompressible case, which we now specify in a simple example. Consider a RT instability occurring in a rectangular tank at rest on a floor, and suppose that the tank is open to the atmosphere, the open end being adjacent to the heavy fluid. As the mixing evolves, the height of the termination of the heavy fluid region must remain stationary (because both fluids are incompressible) and at atmospheric pressure. Since $\partial p_2/\partial z = \rho_2 g$ in the heavy fluid region at all times and p_2 is fixed at a certain height at all times, it follows that p_2 outside the mixing zone is hydrostatic and constant with respect to time; i.e. $p_2 = p_2^h$ in the heavy fluid region, and hence $p_1 \neq p_1^h$ in the light fluid region. We therefore know the value of p_2 at the bubble edge, and p_1 at the spike edge is subsequently determined from Newton's Law, as explained above.

Because the momentum equations are a pair of first-order ODEs, one might expect that their unique solution requires two independent boundary conditions. However, the two boundary conditions specified above are not independent – one of the boundary pressures is derived from the other in conjunction with an integral of the momentum equations, i.e. (4.3). Are the pressure distributions along the mixing zone therefore underspecified? At the limit $A \to 0$, any non-uniqueness is resolved by the

symmetry of the mixing with respect to interchange of the fluids. As $A \to 1$, any non-uniqueness is resolved by the vanishing of fluid 1. At intermediate A, the answer depends on the form of closure used for p^*. This issue is explored in Glimm *et al.* (1998*b*).

4.3. *The centre-of-mass motion of the RT mixing layer*

In § 3.2, we observed that while the net momentum P of the mixing layer increases over time, there is no such restriction on the scaled centre-of-mass position $\widehat{Z}$, and in fact it is possible for $\widehat{Z}$ to be stationary during the entire period of unstable mixing. In this subsection, we discuss the approximate validity of the relation $\widehat{Z} = 0$ for RT mixing.

It is clear that $\widehat{Z}$ should vanish in the symmetric limit ($A \to 0$). For $\widehat{Z}$ to remain zero as A increases, the spikes must become increasingly thin to cancel their favoured mass, but they need not become infinitesimally thin as $A \to 1$, as there is always heavy fluid between the bubbles. This qualitative behaviour has been confirmed in numerical simulations (see, e.g. Gardner *et al.* 1988). Thus $\widehat{Z} = 0$ has a clear physical interpretation and appears to be plausible in an approximate sense.

To compute $\widehat{Z}$ for non-zero A, we require a volume fraction profile (which is implied by a constitutive law for v^*) in addition to values for α_1 and α_2. Equation (3.19) gives $\widehat{Z} = 0$ at $A = 0$ if and only if $\alpha_2 = \alpha_1$, which we know to be true. Evaluating (3.19) at $A = 1$, we have

$$\widehat{Z} = \frac{\alpha_1}{2} \int_0^1 \left[\left(\frac{\widehat{z}}{\alpha_1} \right)^2 - 1 \right] \mathrm{d}\beta_1.$$

The integrand has a single root in the interior of the mixing region, so it is quite possible for $\widehat{Z}$ to be small (relative to α_1), depending on the shape of the volume fraction profile.

Using Youngs' (1989) measurements of α_1 and α_2 and the volume fraction profiles (3.25) implied by the fractional linear model (3.26), we find that (3.19) gives a $\widehat{Z}$ that varies between -0.002 and -0.009 for values of A ranging from 0.79 to 0.93. In other words, $\widehat{Z}$ appears to be solidly an order of magnitude smaller than α_1 at large A. While the precise value of $\widehat{Z}$ is sensitive to the shape of the volume fraction profile, the fact that $\widehat{Z}$ is small is not; any reasonable volume fraction profile gives a similar result.

Conversely, setting $\widehat{Z} = 0$ in the fractional linear model implies a relation between α_2/α_1 and A which correlates well with experimental data. This relation is displayed as the solid curve in figure 4. For comparison, the figure includes the 1989 measurements of Youngs and theoretical predictions based on the two-phase model of Freed *et al.* (1991) and the statistical merger model of Alon *et al.* (1995). Freed *et al.* actually provide two different analytical approximations for α_2/α_1, one for small A and one for large A. Because these approximations do not match at any A, we avoid the problem of how to blend them by showing only the large-A approximation, which pertains to the more interesting region of figure 4 while still being reasonably accurate at small A.

The expansion ratio α_2/α_1 is sensitive to where one terminates the mixing zone. All of the curves shown in figure 4 are for a 0% cutoff, consistent with the method used by Read and Youngs. Freed *et al.* assumed a 5% cutoff when comparing their theoretical expansion ratios to the same experimental data. Increasing the cutoff criterion reduces the expansion ratio; a 5% cutoff would lower the solid curve in

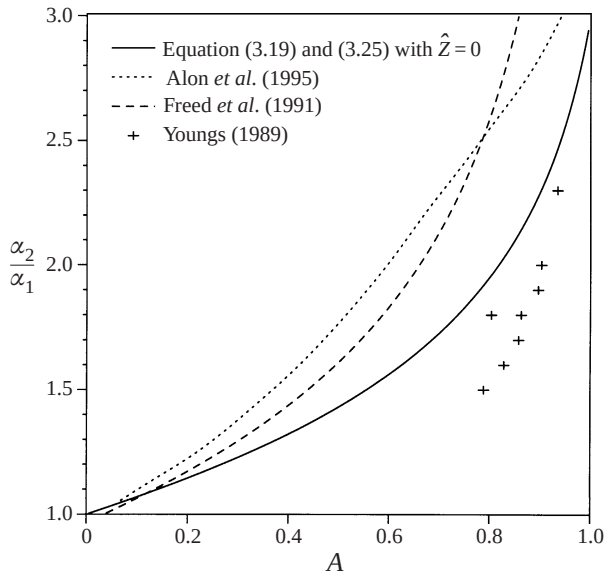

FIGURE 4. The expansion ratio α_2/α_1 of the mixing zone as a function of the Atwood ratio $A = (\rho_2 - \rho_1)/(\rho_2 + \rho_1)$. All of the curves and the experimental data plotted here were obtained assuming sharply-defined mixing zone edges (i.e. no cutoff criterion was applied).

figure 4 enough to make it agree with the experimental data to within the probable uncertainty in the measurements.

We emphasize that the prediction of the expansion ratio implied by setting $\widehat{Z} = 0$ is sensitive to the shape of the volume fraction profile. The correctness of the profiles displayed in figure 3(*a*) has been established only for $A \lesssim 1/3$. Predicting the expansion ratio α_2/α_1 as a function of A amounts to identifying a universal dynamical property of a RT mixing layer, and there are of course numerous ways to search for one. The $\widehat{Z} = 0$ criterion has the advantages that (*a*) it has a clear physical interpretation; (*b*) it is measurable; and (*c*) it is reasonably consistent with the experimental data, based on the comparisons reported above.

4.4. *Comments on new vs. old models for* v^*

The model for v^* that was proposed by Chen *et al.* had $\mu_k = \beta_k$ for $k = 1, 2$, which is the limit of (3.23) as $\alpha_2 \to \alpha_1$. This approximation was validated by comparing the exact and modelled values of $v^* \partial \beta_k / \partial z$ using data from two-dimensional numerical simulations of compressible RT instability. Agreement was good over a fairly wide range of density ratio and compressibility. Since α_2 never greatly exceeds α_1 over the range of A considered by Chen *et al.*, it is not contradictory that this simple model gives good agreement with simulation data in certain contexts, but it should now be considered as a special case of the fractional linear model (3.26).

In Glimm *et al.* (1996), a scale-invariant solution for incompressible RT mixing was presented as a renormalization group fixed point using the original model for v^*. A relation between α_1, α_2, and A was obtained from the two-phase momentum equations with the closure assumptions proposed in Chen *et al.* The expansion ratio α_2/α_1, computed for $\alpha_1 = 0.06$ and variable A, gave reasonable agreement with experiment but tended to underestimate the data. Since this prediction was, in effect, obtained in the $\alpha_2 \to \alpha_1$ limit of (3.23), and it used a hydrostatic approximation for the net

pressure force Δp (valid only at $A = 0$; see § 4.2), it should now be interpreted as a low-A approximation of the solid curve in figure 4.

5. Boundary conditions for Rayleigh–Taylor mixing

Boundary conditions in the form of dynamical equations for the trajectories of the mixing zone edges replace physical and geometrical information that is lost in the averaging process. In RT instability, the furthest penetrating portion of light (heavy) fluid has the shape of a bubble (spike) and it defines the lower (upper) edge of the mixing zone. The geometry of the outer portions of the mixing layer therefore suggests that boundary conditions can be formulated as phenomenological force laws expressing the balance of buoyant, drag, and inertial (added mass) forces on bubbles and spikes, a problem which we discuss in § 5.1. At the same time, force laws can be derived rigorously by combining the two-phase momentum conservation equations and taking one-sided limits. Such laws are identities, permitting arbitrary edge motion, and thus they do not close the system. However, as we will show in § 5.2, they illustrate the important differences between competing two-phase flow models, including their compatibility with phenomenological force laws for bubbles and spikes.

5.1. *Bubble/spike fronts*

Considering a mixing zone edge as a single coherent structure (a leading bubble or spike), we formulate boundary conditions as described above,

$$(\rho_k + \kappa_k \rho_{k'}) \boldsymbol{V}_k \frac{\mathrm{d}V_k}{\mathrm{d}t} = (\rho_k - \rho_{k'}) \boldsymbol{V}_k g - (-1)^k C_k^D \rho_{k'} \boldsymbol{S}_k V_k^2. \tag{5.1}$$

Here, $\boldsymbol{V}_k$ and $\boldsymbol{S}_k$ are, respectively, the total volume and frontal area of the leading bubble ($k = 1$) or spike ($k = 2$); κ_k is an added mass coefficient (which accounts for the increased inertia of the bubble or spike due to its motion through the surrounding fluid) and C_k^D is an adjustable drag coefficient. The form of the drag force in this equation reflects the choice of inertial reference frame in which the fluid infinitely far upstream of the leading bubble or spike is stagnant (see the explanation leading to (3.4) in § 3).

The ratios $\boldsymbol{V}_k/\boldsymbol{S}_k \equiv L_k$ for $k = 1, 2$ introduce phenomenological length scales into the problem. Dividing (5.1) by $\boldsymbol{V}_k$, we get

$$(\rho_k + \kappa_k \rho_{k'}) \frac{\mathrm{d}V_k}{\mathrm{d}t} = (\rho_k - \rho_{k'}) g - (-1)^k \frac{C_k^D \rho_{k'} V_k^2}{L_k}, \tag{5.2}$$

The volume-to-surface ratios L_k represent longitudinal length scales, since the relevant surface is the frontal portion of the leading coherent structure. Otherwise, the precise definition of L_k is problem dependent and somewhat arbitrary.

Dynamical laws similar in form to (5.2) have been used by other authors to study the asymptotic trajectories of bubble and spike fronts in RT instability. This idea was first proposed by Hansom *et al.* in 1990 (also see Youngs 1991). In fact, (5.2) is identical to the model of Hansom *et al.*, up to minor differences in the settings of κ_k and L_k, as explained below. The bubble/spike model of Alon *et al.* (1995) and Alon & Shvarts (1996) contains an adjustable coefficient in the buoyancy term, which is used to obtain consistency with the potential flow model of Layzer (1955). Alon *et al.* have also used their model to analyse the evolution of bubble and spike fronts in the related Richtmyer–Meshkov (RM) instability (shock-wave-induced mixing).

The three bubble/spike models – Hansom *et al.*, Alon *et al.*, and the present one

$$(\rho_k + \kappa_k \rho_{k'}) \frac{\mathrm{d}V_k}{\mathrm{d}t} = C_k^B (\rho_k - \rho_{k'}) g - (-1)^k \frac{C_k^D \rho_{k'} V_k^2}{L_k}$$

Model	L_k	κ_k	C_k^B	C_k^D
Hansom *et al.* (1990)	$\lvert Z_k \rvert$	1	1	$\dfrac{\frac{1}{2} - \alpha_k}{[1-(-1)^k A]\alpha_k}$
Alon *et al.* (1995; 1996)	$\lvert Z_k \rvert$	1	$\frac{1}{2}$	$\dfrac{6\pi}{1+A}$ $(k=1)$ $\dfrac{2\pi}{1-A}\left(\dfrac{4\alpha_1}{\alpha_2} - 1\right)$ $(k=2)$
Present work	$\left\lvert \dfrac{\partial \beta_k}{\partial z} \right\rvert^{-1}_{z=Z_k}$	1 (2D) $\frac{1}{2}$ (3D)	1	$\dfrac{1-2\alpha_k}{[1-(-1)^k A]\alpha_{k'}}$ (2D) $\dfrac{1-2\alpha_k}{[1-(-1)^k A]\alpha_{k'}} + \dfrac{\alpha_k}{2\alpha_{k'}}$ (3D)

TABLE 1. A comparison between three different phenomenological models for the balance of forces on bubble ($k = 1$) and spike ($k = 2$) fronts in RT mixing layers. These models have the common form given above, where κ_k, C_k^B and C_k^D are, respectively, added mass, buoyancy, and drag coefficients. The value of the drag coefficient depends on the convention chosen for the longitudinal length scale L_k, which is indicated in the second column. The settings of κ_k, C_k^B and C_k^D indicated above are relevant to planar incompressible RT mixing, for which the edge trajectories are $Z_k(t) = (-1)^k \alpha_k A g t^2$.

– are compared in table 1. This comparison assumes the asymptotic trajectories (2.9) relevant to incompressible RT instability. The length scale used in the present model is $L_k = |\partial \beta_k / \partial z|^{-1}$, evaluated in the limit of vanishing β_k. Thus L_k depends on the solution for the mixing zone interior. For the incompressible RT mixing layer, L_k is directly obtained from the self-similar solution derived in § 3.2. Differentiating (3.25) we get

$$\frac{\mathrm{d}\widehat{z}}{\mathrm{d}\beta_1} = \frac{2}{\alpha} \left[\alpha_1 \alpha_2 - \widehat{z}(\alpha_1 - \alpha_2)\right].$$

Evaluating this expression at the upper and lower edges of the mixing zone gives

$$L_k(t) = \left| \frac{\partial \beta_k}{\partial z} \right|^{-1}_{\beta_k = 0} = \frac{\mathrm{d}\widehat{z}}{\mathrm{d}\beta_1} \Big|_{\beta_k = 0} \mathscr{Z}(t) = \frac{2\alpha_k^2}{\alpha_{k'}} A g t^2. \tag{5.3}$$

The reason for this somewhat complicated choice of L_k will be made clear below. The setting of the added mass coefficient κ_k depends on the front geometry. In two (three) dimensions, we approximate the bubble/spike front as having a circular (spherical) profile, so that $\kappa_k = 1$ ($\kappa_k = 1/2$) (Lamb 1932). Hansom *et al.* and Alon *et al.* both use $L_k = |Z_k|$ and $\kappa_k = 1$. In the large-time limit of the expanding RT mixing layer, the buoyancy coefficient C_k^B in the Alon *et al.* model approaches $1/2$.

Inserting the trajectories (2.9) into the bubble/spike evolution equations (5.2) for $k = 1, 2$ determines a map between the mixing coefficients (α_1, α_2) and the drag coefficients (C_1^D, C_2^D). These relations are given for the three models in table 1. Since the boundary conditions for incompressible RT instability are already known up to

determination of the mixing coefficients α_1 and α_2, the phenomenological boundary conditions (5.2) are useful only to the extent that they are valid outside of this flow regime, e.g. to compressible fluids or to RM mixing. For example, Alon *et al.* (1995) and Alon & Shvarts (1996) used known results for incompressible RT mixing to set the coefficients in their bubble/spike model, and then found that it gave an accurate prediction of the mixing layer growth rates in RM mixing.

In our judgment, the similarities between these models are more important than the differences. Further work should address the validation and calibration of these models for other flow regimes, including the problem of setting the phenomenological coefficients.

5.2. *Two-phase limits*

Force balances for the mixing zone edges can be derived rigorously from a two-phase flow model by combining the momentum equations and taking one-sided limits. We now demonstrate this procedure using the momentum equations written in the general form

$$\rho_k \frac{\mathrm{D}_k v_k}{\mathrm{D}t} = -\frac{\partial p_k}{\partial z} + \rho_k g + \frac{f_{kk'}}{\beta_k}, \tag{5.4}$$

where $\mathrm{D}_k/\mathrm{D}t \equiv \partial/\partial t + v_k \partial/\partial z$ is the phase-k convective derivative and $f_{kk'}$ is a general interfacial source term, which in the absence of single-phase turbulence is given by

$$f_{kk'} = (p^* - p_k)\frac{\partial \beta_k}{\partial z}.$$

We now consider incompressible flow and compare the present model to the single-pressure model of Freed *et al.* (1991), which is based on earlier single-pressure two-phase flow models (Harlow & Amsden 1975; Youngs 1984). Assuming the model (2.6) for p^* introduced in § 1,

$$f_{kk'} = \mu_k^p(t, \beta_k)(p_{k'} - p_k)\frac{\partial \beta_k}{\partial z}. \tag{5.5}$$

Denoting quantities specific to the Freed model with a superscript F, we have

$$f_{kk'}^F = -(-1)^k \frac{C^F \beta_1 \beta_2 \rho}{L^F}(v_2 - v_1)^2, \tag{5.5F}$$

where C^F and L^F are, respectively, a phenomenological drag coefficient and mixing length for the interior of the mixing zone, and $\rho = \beta_1\rho_1 + \beta_2\rho_2$. The mixing length L^F satisfies its own evolution equation, given in Freed *et al.* (1991).

At edge k, which follows the trajectory $z = Z_k(t)$, we have $\beta_k = 0$, $\beta_{k'} = 1$, $v_{k'} = 0$, and $v_k = V_k$. Consider the acceleration $\mathrm{D}_{k'}v_{k'}/\mathrm{D}t$ of the ambient phase at this edge, which in view of these boundary conditions is equal to $\partial v_{k'}/\partial t$. However, because edge k is a phase-k particle characteristic,

$$0 = \frac{\mathrm{D}_k v_{k'}}{\mathrm{D}t} = \frac{\partial v_{k'}}{\partial t} + V_k \frac{\partial v_{k'}}{\partial z},$$

so that

$$\frac{\mathrm{D}_{k'} v_{k'}}{\mathrm{D}t} = -V_k \frac{\partial v_{k'}}{\partial z}$$

along $z = Z_k(t)$. Expanding the derivative in the incompressiblity condition (3.3),

$$\beta_k \frac{\partial v_k}{\partial z} + v_k \frac{\partial \beta_k}{\partial z} + \beta_{k'} \frac{\partial v_{k'}}{\partial z} + v_{k'} \frac{\partial \beta_{k'}}{\partial z} = 0.$$

Evaluation of this expression at edge k yields $\partial v_{k'}/\partial z = -V_k \partial \beta_k/\partial z$; thus

$$\frac{\mathrm{D}_{k'} v_{k'}}{\mathrm{D}t} = V_k^2 \frac{\partial \beta_k}{\partial z}. \tag{5.6}$$

By subtracting the k' from the k momentum equation (5.4), evaluating along $z = Z_k(t)$, and using (5.6), we derive dynamical equations for the mixing zone edges,

$$\rho_k \frac{\mathrm{d}V_k}{\mathrm{d}t} = (\rho_k - \rho_{k'})g + \frac{\partial}{\partial z}(p_{k'} - p_k) - (-1)^k \frac{\rho_{k'} V_k^2}{L_k} - f_{k'k} + \lim_{\beta_k \to 0} \frac{f_{kk'}}{\beta_k}. \tag{5.7}$$

The length scales L_k given by (5.3) appear naturally in these equations, due to the inertia of the ambient phase at a mixing zone edge. This fact has nothing to do with the modelling of the interfacial force $f_{kk'}$. Substitution of both models for $f_{kk'}$, (5.5) and (5.5F), into (5.7) gives

$$\rho_k \frac{\mathrm{d}V_k}{\mathrm{d}t} = (\rho_k - \rho_{k'})g + \frac{\partial}{\partial z}(p_{k'} - p_k) - \frac{(-1)^k}{L_k}\left[\rho_{k'} V_k^2 + (v_k - 1)(p_{k'} - p_k)\right] \tag{5.8}$$

and

$$\rho_k \frac{\mathrm{d}V_k}{\mathrm{d}t} = (\rho_k - \rho_{k'})g - (-1)^k \left(\frac{1}{L_k} + \frac{C^F}{L^F}\right) \rho_{k'} V_k^2, \tag{5.8F}$$

respectively, where $v_k(t) = \lim_{\beta_k \to 0} \mu_k^p(t, \beta_k)/\beta_k$ and in (5.8F) we have set $p_2 = p_1$.

It is important to understand that equations (5.7) for $k = 1, 2$ do not replace the boundary conditions for the mixing zone edges, e.g. (5.2). Because (5.7) is derived from the momentum equations, which are first-order ODEs, it certainly cannot supply the independent boundary data required to uniquely specify the two-phase flow. However, (5.7) helps to separate out the forces that act on the bubble/spike fronts, so that it is worthwhile to compare (5.8) and (5.8F) to the 'general' phenomenological equation displayed at the top of table 1. In view of the step leading from (5.1) to (5.2), we identify the terms in (5.8) and (5.8F) as volume or surface forces, the latter being proportional to an inverse length scale. This partitioning of the forces leads to some interesting observations and raises new questions about the phenomenological modelling of the bubble/spike fronts.

Note that the buoyant force density $(\rho_k - \rho_{k'})g$ appears in (5.8) and (5.8F) with a coefficient of unity ($C_k^B = 1$). This does not mean that it is incorrect to readjust buoyancy, but the source of the readjustment should be another volume force, for example the pressure difference gradient in (5.8). The Freed model lacks the degrees of freedom to describe a readjusted buoyant force, and is thus incompatible with any front equations having $C_k^B \neq 1$. A similar remark applies to the added mass $\kappa_k \rho_{k'} \mathrm{d}V_k/\mathrm{d}t$. Equation (5.8F) lacks a term to account for this volume force, while again the pressure difference gradient in (5.8) is a possible source of added mass.

Despite its definition and appearance as such, $f_{kk'}$ is not strictly a surface force. An alternative model for p^* could have a term proportional to a length; its contribution to $f_{kk'}$ through $p^* \mathrm{d}\beta_k/\mathrm{d}z$ would therefore be a volume force. In a dispersed two-phase flow, $p^* \mathrm{d}\beta_k/\mathrm{d}z$ does in fact contribute a volume force, in the form of added mass (Stuhmiller 1977). Addition of such a term to a model for $f_{kk'}$ would add a term to the right-hand side of (5.8) similar to the added mass term in the phenomenological law (5.2). The issue of whether p^* should be modified to include added mass leads to a larger question of whether the regions near the edges of the mixing layer (where one of the volume fractions is small) can be correctly described by conventional dispersed two-phase flow models. These issues deserve further study.

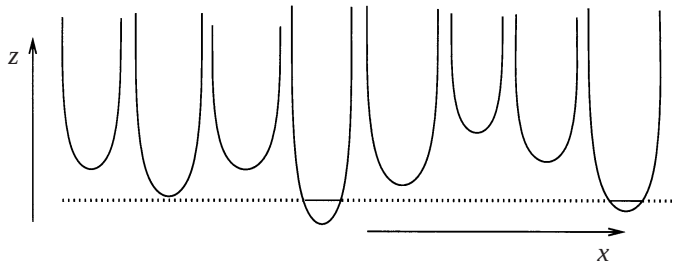

FIGURE 5. Horizontal averaging at a height near the tips of the leading bubbles, where $\beta_1 \approx 0$. Contributions to phase 1 quantities come from the solid segments, all of which lie near bubble tips. Contributions to phase 2 quantities come from the dotted segments, which occur in a variety of flow regimes.

6. Two-pressure vs. single-pressure two-phase flow models

The results of the previous sections indicate that several important properties of the evolution of an incompressible mixing layer are determined from a single constitutive law. Depending on the form of boundary closure assumed (i.e. whether or not it involves pressure), the coupling of the momentum equations to the interface and continuity equations can occur only at the edges of the mixing zone. This situation breaks down in mixing processes where compressibility is important. We therefore explain the reasons why the two-pressure formulation of two-phase mixing has a sounder physical and mathematical foundation than one with a single pressure field.

A two-phase flow of immiscible fluids can be interpreted as a statistical average over an ensemble of microscopic flow realizations. In this picture, two-phase models that utilize a single pressure field impose a constraint of local pressure equilibration on the averaged flow, i.e. $p_1 = p_2$ everywhere inside the mixing layer. This assumption is physically implausible, as the following argument shows.

Consider a two-dimensional RT problem with an arbitrarily long array of random modes arranged along the horizontal (x) direction. In this example, one obtains a single-phase quantity by horizontally averaging. In particular, $p_1(z,t)$ is the average value of the local pressure p, at fixed z and t, over all x where the light fluid is present. Suppose that the value of z is close to the displacement of the leading bubble tips, as illustrated in figure 5. Then the contributions to the sample of light fluid determining p_1 (the solid segments in figure 5) are in general widely spaced and they primarily belong to a single flow regime, the flow near a bubble tip. On the other hand, to compute p_2 at the same height, one samples the heavy fluid in different flow regimes, as the regions of heavy fluid across which one is averaging (the dotted segments in figure 5) are at widely varying distances from bubble tips. While the microscopic (pre-averaged) fluid pressures are roughly equal near the bubble tips, the regions near the leading bubble tips make the dominant contribution to p_1 but not to p_2. Thus it is not physically reasonable to impose the constraint $p_1 = p_2$. The same argument applied to the other side of the mixing zone explains why equilibration of the average pressures does not occur near the tips of the leading spikes.

The pressures p_1 and p_2 do not equilibrate in the interior of the mixing zone, for reasons that are fundamentally the same but have a different explanation. The heavy (light) fluid in the microscopic flow is primarily contained within spikes (bubbles), a fact which biases the averaging process to determine the single-phase pressure. At any height within the mixing layer, there are significant pressure differences between spikes and bubbles on the basis of hydrostatics and inertial forces, so that $p_1 \neq p_2$ in

general. Non-equilibration of pressure in RT instability is easy to understand in the case $A = 1$, for then p_1 is identically zero everywhere while p_2 cannot possibly satisfy this constraint throughout the mixing zone.

Imposing pressure equilibration rules out a possibly important mode of interphase momentum transfer. The form of $f_{kk'}$ given by (5.5) indicates that the drag force in the interior of the mixing layer is purely a pressure drag, but our model is compatible with other forms of drag. Two-phase flow models with equal fluid pressures cannot describe a drag force based on pressure differences. A viscous drag law such as (5.5F) is often used to model the momentum exchange in single-pressure two-phase models (see, e.g. Drew 1983; Harlow & Amsden 1975; Youngs 1984).

There are several more reasons not to set $p_2 = p_1$. On a mathematical basis, two-pressure models have real characteristic values (Stewart & Wendroff 1984; Holm & Kupershmidt 1984; Ransom & Hicks 1984), and thus can be solved using standard numerical techniques for hyperbolic partial differential equations. Ransom & Hicks (1984) have studied this issue in detail and concluded that imposing pressure equilibration in a two-phase separated flow introduces instabilities which lack a physical basis and, even worse, may obscure the actual (physical) instabilities. It is also difficult to formulate an equation of state for a two-phase compressible flow with a single pressure field unless one assumes that the fluids mix at the molecular level. Fundamentally, $p_2 = p_1$ is a modelling approximation, used to close the equations of motion, and its validity or lack of validity must be determined by reference to the physics of the specific problem. In contrast, distinct pressures appear naturally in the ensemble-averaged equations of motion, which are formally exact. Thus the two-pressure formulation offers compelling improvements in the modelling of two-phase immiscible fluid mixing.

7. Conclusion

In this study, we have improved and extended a two-phase flow model for the macroscopic evolution of chaotic fluid mixing, with an emphasis on its application to Rayleigh–Taylor instability. The principal features that distinguish the two-phase flow model proposed here from other models (Harlow & Amsden 1975; Youngs 1984; Freed *et al.* 1991) are the following: The present model

(*a*) describes compressible fluids, and thus requires boundary conditions for the edges of the mixing zone (the equivalent boundary conditions in the incompressible limit are the trajectories $Z_k(t) = (-1)^k \alpha_k A g t^2$);

(*b*) is compatible with all known models for the forces on the leading bubbles and spikes in Rayleigh–Taylor instability;

(*c*) contains distinct pressure fields, one for each phase, and thus allows for interphase momentum transfer via pressure forces;

(*d*) utilizes an ensemble-averaged kinematic equation for the material interface, which is a hyperbolic equation for the volume fraction. The modelling of the propagation speed v^* replaces the more common closure approximation $p_2 = p_1$.

Other potentially important processes, such as viscous drag, mass diffusion, turbulent diffusion, and heat conduction, can be incorporated into the model in a straightforward manner.

The work of J.G. and D.S. is supported by the Applied Mathematics Subprogram of the US Department of Energy, DE-FG02-90ER25084. J.G. is also supported by the Army Research Office, grant DAAH04-95-10414, and the National Science

Foundation, grant DMS-95-00568. D.H.S. is supported by the US Department of Energy.

REFERENCES

Alon, U., Hecht, J., Ofer, D. & Shvarts, D. 1995 Power laws and similarity of Rayleigh–Taylor and Richtmyer–Meshkov mixing fronts at all density ratios. *Phys. Rev. Lett.* **74**, 534–538.

Alon, U. & Shvarts, D. 1996 Two-phase flow model for Rayleigh–Taylor and Richtmyer–Meshkov mixing. In *Proc. the Fifth Intl Workshop on Compressible Turbulent Mixing* (ed. R. Young, J. Glimm & B. Boston). World Scientific.

Chen, Y. 1995 Two phase flow analysis of turbulent mixing in the Rayleigh–Taylor instability. PhD thesis, State University of New York at Stony Brook.

Chen, Y., Deng, Y., Glimm, J., Li, G., Sharp, D. H. & Zhang, Q. 1993 A renormalization group scaling analysis for compressible two-phase flow. *Phys. Fluids* A **5**, 2929–2937.

Chen, Y., Glimm, J., Sharp, D. H. & Zhang, Q. 1996 A two-phase flow model of the Rayleigh–Taylor mixing zone. *Phys. Fluids* **8**, 816–825.

Cranfill, C. W. 1991 A multifluid turbulent-mixing model. *Tech. Rep.* LA-UR-91-403. Los Alamos National Laboratory.

Cranfill, C. W. 1992 A new multifluid turbulent-mixing model. *Tech. Rep.* LA-UR-92-2484. Los Alamos National Laboratory.

Drew, D. A. 1983 Mathematical modeling of two-phase flow. *Ann. Rev. Fluid Mech.* **15**, 261–291.

Freed, N., Ofer, D., Shvarts, D. & Orszag, S. 1991 Two-phase flow analysis of self-similar turbulent mixing by Rayleigh–Taylor instability. *Phys. Fluids* A **3**, 912–918.

Gardner, C. L., Glimm, J., McBryan, O., Menikoff, R., Sharp, D. & Zhang, Q. 1988 The dynamics of bubble growth for Rayleigh–Taylor unstable interfaces. *Phys. Fluids* **31**, 447–465.

Glimm, J., Li, X.-L., Menikoff, R., Sharp, D. H. & Zhang, Q. 1990 A numerical study of bubble interactions in Rayleigh–Taylor instability for compressible fluids. *Phys. Fluids* A **2**, 2046–2054.

Glimm, J., Saltz, D. & Sharp, D. H. 1996 Renormalization group solution of two-phase flow equations for Rayleigh–Taylor mixing. *Phys. Lett.* A **222**, 171–176.

Glimm, J., Saltz, D. & Sharp, D. H. 1998*a* The statistical evolution of chaotic fluid mixing. *Phys. Rev. Lett.* **80**, 712–715.

Glimm, J., Saltz, D. & Sharp, D. H. 1998*b* Two-pressure two-phase flow. In *Nonlinear Partial Differential Equations* (ed. G.-Q. Chen, Y. Li & X. Zhu). World Scientific.

Glimm, J. & Sharp, D. H. 1990 Chaotic mixing as a renormalization group fixed point. *Phys. Rev. Lett.* **64**, 2137–2139.

Hansom, J. C. V., Rosen, P. A., Goldack, T. J., Oades, P. F. K., Cowperthwaite, N., Youngs, D. L., Mawhinney, N. & Baxter, A. J. 1990 Radiation driven planar foil instability and mix experiments at the AWE HELEN laser. *Laser and Particle Beams* **8**, 51–71.

Harlow, F. & Amsden, A. 1975 Flow of interpenetrating material phases. *J. Comput. Phys.* **18**, 440–464.

Holm, D. & Kupershmidt, B. 1984 Multipressure regularization for multiphase flow. *Phys. Lett.* A **106**, 165–168.

Lamb, H. 1932 Hydrodynamics. Dover.

Layzer, D. 1955 On the instability of superimposed fluids in a gravitational field. *Astrophys. J.* **122**, 1–12.

Menikoff, R. & Plohr, B. 1989 The Riemann problem for fluid flow of real materials. *Rev. Mod. Phys.* **61**, 75–130.

Ransom, V. H. & Hicks, D. L. 1984 Hyperbolic two-pressure models for two-phase flow. *J. Comput. Phys.* **53**, 124–151.

Read, K. I. 1984 Experimental investigation of turbulent mixing by Rayleigh–Taylor instability. *Physica* D **12**, 45–58.

Sharp, D. H. 1984 An overview of Rayleigh–Taylor instability. *Physica* D **12**, 3–18.

Snider, D. M. & Andrews, M. J. 1994 Rayleigh–Taylor and shear driven mixing with an unstable thermal stratification. *Phys. Fluids* **6**, 3324–3334.

Stewart, H. B. & Wendroff, B. 1984 Two-phase flow: Models and methods. *J. Comput. Phys.* **56**, 363–409.

STUHMILLER, J. H. 1977 The influence of interfacial pressure forces on the character of two-phase flow model equations. *Intl J. Multiphase Flow* **3**, 551–560.

YOUNGS, D. L. 1984 Numerical simulation of turbulent mixing by Rayleigh–Taylor instability. *Physica* D **12**, 32–44.

YOUNGS, D. L. 1989 Modeling turbulent mixing by Rayleigh–Taylor instability. *Physica* D **37**, 270–287.

YOUNGS, D. L. 1991 Three-dimensional numerical simulation of turbulent mixing by Rayleigh–Taylor instability. *Phys. Fluids* A **3**, 1312–1319.